

## Thermoelastic Properties of MgSiO<sub>3</sub>-Perovskite: Insights on the Nature of the Earth's Lower Mantle

R. M. Wentzcovitch,<sup>1,2</sup> B. B. Karki,<sup>3</sup> M. Cococcioni,<sup>2</sup> and S. de Gironcoli<sup>2</sup>

<sup>1</sup>*Department of Chemical Engineering and Materials Science, Minnesota Supercomputing Institute, University of Minnesota, Minneapolis, Minnesota 55455, USA*

<sup>2</sup>*Scuola Internazionale Superiore di Studi Avanzati (SISSA) and INFN-DEMOCRITOS National Simulation Center, I-34014 Trieste, Italy*

<sup>3</sup>*Department of Computer Science, Louisiana State University, Baton Rouge, Louisiana 70803, USA*  
(Received 14 April 2003; published 9 January 2004)

We have determined by means of first principles quasiharmonic calculations the elastic constants and acoustic velocities of MgSiO<sub>3</sub> perovskite, the most abundant mineral of the Earth's lower mantle (LM), at pertinent pressures and temperatures. Using these results, along with the effects of low concentration iron alloying and the thermoelasticity of the most important secondary LM phase, MgO, we predict the isotropic elastic moduli of likely LM aggregates. Comparison with seismic values extracted from the preliminary reference Earth model indicates that the top of the LM behaves as a typical aggregate of pyrolytic composition, likewise the upper mantle. But systematic deviations that cannot be accounted for by alterations in the geotherm alone develop toward the deep LM. This result could be viewed as evidence in support of radially inhomogeneous LM models.

DOI: 10.1103/PhysRevLett.92.018501

PACS numbers: 91.35.-x, 31.15.Ar, 62.20.Dc, 74.25.Kc

First principles calculations of structural [1] and thermodynamic [2–4] properties of complex earth forming minerals have emerged in the last decade as a powerful addition to experimental high pressure techniques in mineral physics. Although experimental progress has been steady [5,6], elasticity measurements at lower mantle conditions still pose considerable challenges. Here we report the single crystal and aggregate elasticity of MgSiO<sub>3</sub> perovskite, the most abundant mineral in the Earth (perhaps ≈55% in mass). It exists in the lower mantle (LM) and its properties determine, to a great extent, the properties of this region. The LM is the largest continuous region of the planet extending from ≈670 to 2890 km of depth, where thermodynamic conditions vary from about 23 GPa and ≈1900 K to 135 GPa and maybe ≈4000 K [7]. These elastic constants are used to predict acoustic velocities of hypothetical LM mineral aggregates. Comparison with observed seismic velocities in this region [8] are then made to test standard homogeneous mineralogical LM models and elucidate the present state of this layer. This information is necessary to resolve, among other things, the style of thermochemical convection operating in the mantle today [9,10].

Our approach [2] exploits the volume and strain dependence of the vibrational frequencies to determine the thermal contribution to the free energy within the quasiharmonic approximation (QHA). The elastic constants shown in Fig. 1 were obtained by computing the isothermal ones,  $c_{ij}^T(P, T) = [\frac{\partial^2 G(P, T)}{\partial \epsilon_i \partial \epsilon_j}]_P$ , and converting them to adiabatic:  $c_{ij}^S(P, T) = c_{ij}^T(P, T) + \frac{VT\lambda_i \lambda_j}{C_V}$ , where  $\lambda_i(P, T) = [\frac{\partial S(P, T)}{\partial \epsilon_i}]_P$  ( $G$  = Gibbs free energy,  $\epsilon_i$  = strains,  $V$  = volume,  $C_V$  = specific heat,  $S$  = entropy). The basic de-

tails of this calculation are the same as those reported previously [3] (see [11], Fig. 1, and Table I captions). Experimental validation of these results is possible only at ambient conditions for which there are ultrasonic [6] and Brillouin [5] measurements. Table I shows that differences between calculated and measured elastic constants are relatively small and nonsystematic (see [11], Fig. 1, and Table I captions). This is reflected in the good agreement between calculated and measured aggregate moduli [16],  $K_S$  and  $G$ , which averages out individual discrepancies. The values of predicted properties are nearly independent of the order used in the finite strain expansion of the free energy (third or fourth order) [3] as long as these are restricted to the  $(P, T)$  range of validity of the QHA. The latter has been determined by disregarding results beyond which  $[\frac{\partial^2 \alpha(P, T)}{\partial T^2}]_P \geq 0$  at high  $T$ 's,  $\alpha(P, T)$  being the thermal expansion coefficient [3].  $\partial G / \partial T$  at ambient conditions is  $-0.026$  GPa/K, similar to the values obtained by ultrasonic shear velocity measurements [6],  $-0.029(3)$  GPa/K. This range of values suggested [17] (a) a pyrolytic composition for the LM [ $\approx 80\%$  (Mg<sub>(1-x)</sub>, Fe<sub>x</sub>)SiO<sub>3</sub> and  $20\%$  (Mg<sub>(1-y)</sub>, Fe<sub>y</sub>)O] and that (b) thermoelastic effects alone can account to a great extent for the observed lateral variations of seismic velocities [17]. The present calculation supports the latter view, which will be fully explored somewhere else. Here we address the former assertion only.

Figure 1 displays our elastic constants and those calculated by Oganov *et al.* [4] using molecular dynamics. In principle both approaches are equivalent but, in addition, theirs accounts fully for anharmonic effects (intrinsic  $T$  effects). On the other hand, the limited sampling of configuration space determined by the 80 atom

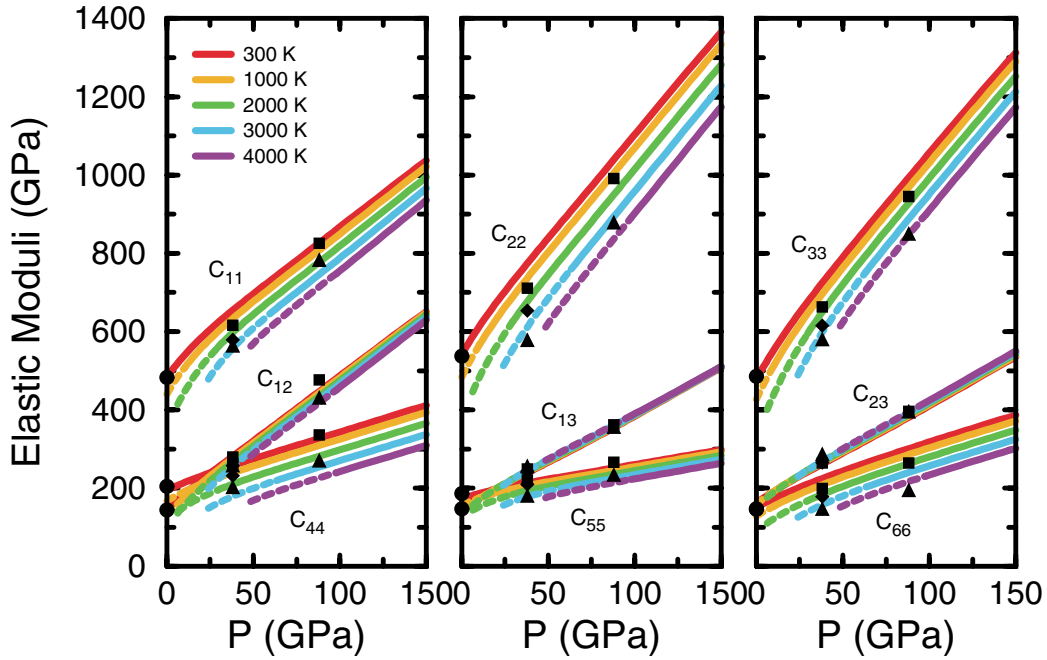


FIG. 1 (color). Pressure dependence of the adiabatic elastic constants of  $\text{MgSiO}_3$ . The line's thickness represents uncertainties caused mainly by the use of the local density approximation (LDA) (see [11]). Full (dashed) lines correspond to results within (outside) the  $(P, T)$  regime of validity of the QHA. Measurements are represented by full circles at 0 GPa [5]. Full symbols at  $P > 0$  GPa are the results of Oganov *et al.* [4] at 38 and 88 GPa (squares: 1500 K, diamonds: 2500 K, up triangles: 3500 K).

simulation implies in larger statistical uncertainties (our calculation is equivalent to a 1280 atom simulation). Their results (see the Fig. 1 caption) obtained at pressures corresponding to 1000 and 2000 km depth are in quite good agreement with ours, with some discrepancies in  $C_{11}$ ,  $C_{12}$ ,  $C_{44}$ , and  $C_{66}$ . Figure 2(a) displays predicted velocities and density,  $\rho$ , for  $\text{MgSiO}_3$  and compares them with seismic [Preliminary Reference Model (PREM)] values [8].  $\rho$  is an insensitive quantity, changing by  $\approx 1\%$  after a variation of 1000 K at conditions at the bottom of the LM. This is approximately the uncertainty in  $\rho^{\text{PREM}}$  and a

reason for not attempting to compare predicted and observed  $\rho$ 's to infer the thermochemical state of the LM.  $V_P^{\text{PREM}}$  crosses several isotherms of  $V_P$ , suggesting  $\Delta T \approx 2000$  K from top to bottom in the LM, if it consisted 100% of  $\text{MgSiO}_3$ .  $V_S^{\text{PREM}}$ , on the other hand, agrees closely with the 2500 K isotherm of  $V_S$ .

Figure 2(b) shows that our aggregate moduli and those obtained by Oganov *et al.* [4] are in good agreement. Random deviations in individual elastic constants are averaged away. More relevant is the similarity in pressure and temperature gradients,  $K_S'$ ,  $G'$ ,  $\partial G/\partial T$ , and  $\partial K_S/\partial T$ ,

TABLE I. Adiabatic elastic constants, wave velocities, and pressure and temperature derivatives of  $\text{MgSiO}_3$ : results at ambient conditions (1) shifted by  $P = 5$  GPa (see [11]) and (1\*) unshifted; (2) range of values obtained in static density functional theory calculations ([18,19], and references therein), including this one; (3) experimental values obtained by Brillouin [5] and (+) ultrasonic [6] measurements; (4) at ambient conditions (shifted by 5 GPa) and at (4') 300 K and 100 GPa (shifted by 5 GPa). Pressure and elastic constants in GPa, velocities in km/s, temperature in K.

|  | $c_{11}$ | $c_{22}$ | $c_{33}$ | $c_{44}$ | $c_{55}$ | $c_{66}$ | $c_{12}$ | $c_{13}$ | $c_{23}$ | $K_S$    | $G$                   | $V_P$    | $V_S$                   |
|--|----------|----------|----------|----------|----------|----------|----------|----------|----------|----------|-----------------------|----------|-------------------------|
| (1) $M$                                  | 484      | 542      | 477      | 195      | 172      | 151      | 146      | 146      | 162      | 267      | 173                   | 10.97    | 6.46                    |
| (1*) $M$                                 | 449      | 500      | 434      | 183      | 162      | 138      | 123      | 129      | 144      | 241      | 161                   | 10.60    | 6.30                    |
|  | 491      | 560      | 474      | 203      | 186      | 153      | 134      | 144      | 156      | 263      | 179                   | 10.94    | 6.53                    |
| (2) $M$                                  | $\vdots$              | $\vdots$ | $\vdots$                |
|  | 477      | 524      | 456      | 198      | 173      | 145      | 128      | 135      | 144      | 257      | 175                   | 10.89    | 6.51                    |
| (3) $M$                                  | 482      | 537      | 485      | 204      | 186      | 147      | 144      | 147      | 146      | 264      | 177; 175 <sup>+</sup> | 11.04    | 6.57; 6.56 <sup>+</sup> |
| (4) $\partial M/\partial P$              | 6.3      | 7.5      | 8.2      | 2.2      | 1.7      | 2.4      | 4.2      | 3.0      | 3.3      | 4.8      | 2.0                   | 0.060    | 0.026                   |
| (4') $\partial M/\partial P$             | 3.4      | 5.3      | 5.2      | 1.4      | 0.8      | 1.4      | 3.3      | 2.4      | 2.5      | 3.4      | 1.0                   | 0.021    | 0.008                   |
| (4) $\partial M/\partial T$              | -0.046   | -0.064   | -0.054   | -0.032   | -0.016   | -0.026   | -0.013   | -0.001   | 0.000    | -0.021   | -0.026                | -0.0003  | -0.0002                 |
| (4') $\partial M/\partial T$             | -0.018   | -0.033   | -0.022   | -0.022   | -0.006   | -0.016   | -0.004   | 0.002    | 0.005    | -0.014   | -0.020                | -0.0001  | -0.0001                 |
| (4) $\partial^2 M/\partial P \partial T$ | -0.017   | -0.016   | -0.016   | -0.0005  | -0.0005  | -0.004   | -0.006   | -0.006   | -0.007   | 0.00075  | 0.00052               | 0.000020 | 0.000012                |

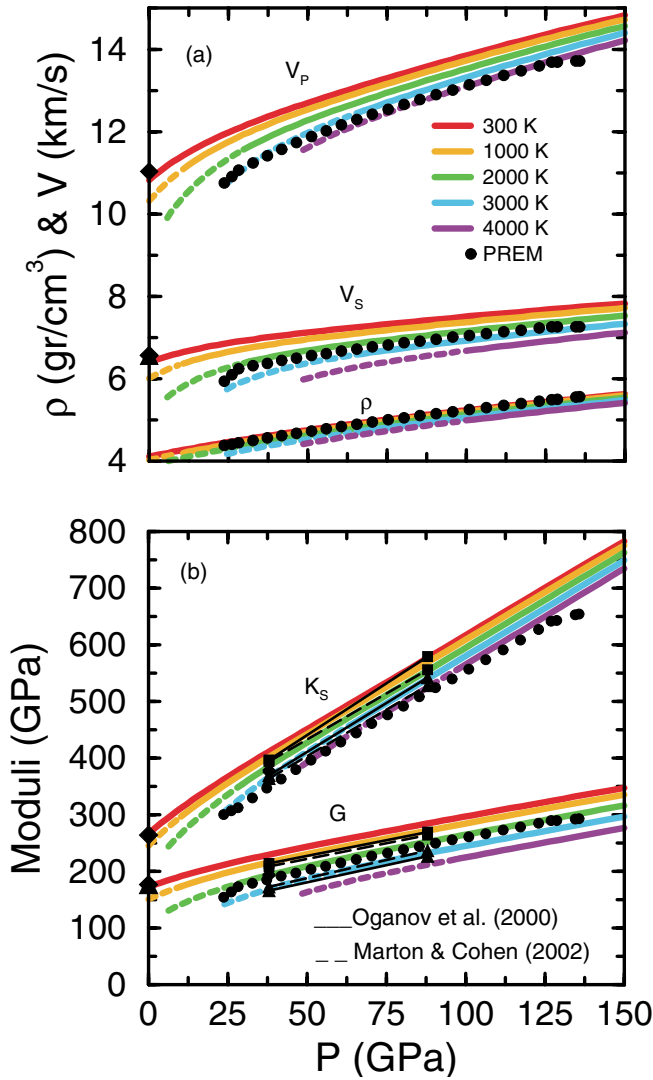


FIG. 2 (color). Pressure dependence of (a) density,  $\rho$ , and isotropic longitudinal [ $V_p = \sqrt{(K_s + 4G/3)/\rho}$ ] and shear ( $V_s = \sqrt{G/\rho}$ ) wave velocities of  $\text{MgSiO}_3$ ; (b) isothermal bulk ( $K_s$ ) and shear ( $G$ ) moduli. Symbols connected by full and dashed black lines are the results of Oganov *et al.* [4] and Marton and Cohen [12], respectively. The gradients obtained in the three calculations depicted in this figure are cited at the midpoints between extreme  $P$ 's and  $T$ 's considered [ $M'(T) = \frac{\partial M(63,T)}{\partial P}$  and  $\hat{M}(P) = \frac{\partial M(P,2500)}{\partial T}$ ]. They are cited in the following order: this work, [4], and [12].  $K'_s(1500) = 3.32, 3.64, 3.24$ ;  $K'_s(3500) = 3.41, 3.41, 3.28$ ;  $G'(1500) = 1.13, 0.88, 1.10$ ;  $G'(3500) = 1.14, 1.12, 1.28$ ;  $\hat{K}_s(38) = -0.019, -0.014, -0.015$  GPa/K;  $\hat{K}_s(88) = -0.014, -0.018, -0.014$  GPa/K;  $\hat{G}(38) = -0.024, -0.024, -0.018$  GPa/K;  $\hat{G}(88) = -0.021, -0.029, -0.014$  GPa/K. Brillouin and ultrasonic measurements are represented by diamonds [5] and up triangles [6], respectively, at  $P = 0$  GPa. Full circles are PREM data [8].

which are the basis for an important insight, hinted earlier [3] but fully derived here, regarding the homogeneity of the LM (see below). Figure 2(b) also displays the aggregate moduli obtained using the potential induced breathing method and variable cell shape molecular dy-

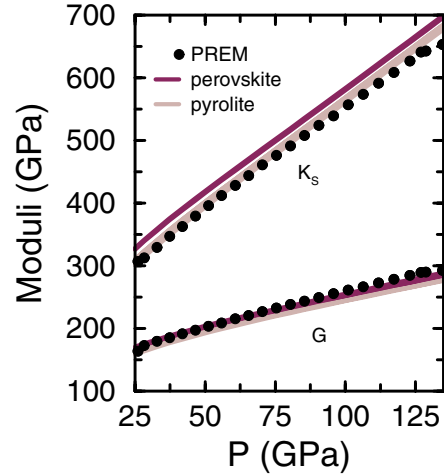


FIG. 3 (color). Bulk ( $K_s$ ) and shear ( $G$ ) moduli for  $(\text{Mg}_{(1-x)}, \text{Fe}_x)\text{SiO}_3$ -pv and pyrolite with  $20\% < V_{mw} < 30\%$  ( $m_w = \text{Mg}_{(1-y)}, \text{Fe}_y\text{O}$ ) along the Brown and Shankland geotherm [13].  $0.0 < x < 0.12$  and  $1 < y/x < 4$ . The effect of Fe on the elastic moduli of pv and mw were extracted from [19,20], respectively.

namics [12]. The agreement with those results is also reasonable; however, there are subtle but important differences on  $K'_s$  and  $\partial G/\partial T$  (see below). Figure 2(b) shows that  $K_s^{\text{PREM}}$  crosses several isotherms such as  $V_p^{\text{PREM}}$ . This trend had already been revealed by our calculations of the single crystal isotropic compressibility of  $\text{MgSiO}_3$  [3] and by an earlier extrapolation of a combination of first principles results at  $T = 0$  K and high  $T$  experimental data [14] to LM conditions [15]. Like  $V_p^{\text{PREM}}$ ,  $G^{\text{PREM}}$  also seems to agree closely to the 2500 K isotherm of  $G$ , another consequence of the insensitivity of  $\rho$ . Since *static* elasticity calculations are in close agreement (see Table I and [18]) and first principles high  $T$  calculations performed to date [3,4] reveal similar trends for  $K_s$ , it seems that the trends once again revealed here for  $K_s$  are robust, reproducible, and might be meaningful. Now we also have detailed results for  $G$ ,  $G'$ , and  $\partial G/\partial T$ . Calculations by Oganov *et al.* [4] for a few  $P, T$ 's offer consistent gradients for both moduli (see the Fig. 2(b) caption). In fact their isothermal pressure gradients for  $K_s$  and  $G$  are slightly larger and smaller, respectively (see Fig. 2(a)), which would enhance the observed trends and further support the insight we are about to derive.  $K'_s$ 's and  $\partial G/\partial T$ 's by Marton and Cohen are somewhat smaller and seem to lead to different conclusions [12].

Figure 3 displays  $K_s$  and  $G$  for isotropic and homogeneous mineralogical models along a standard adiabatic geotherm [13] that nearly coincides with the isentropes of  $\text{MgSiO}_3$  and  $\text{MgO}$  [2,3]. The mineralogical models are pure perovskite,  $(\text{Mg}_{(1-x)}, \text{Fe}_x)\text{SiO}_3$ , with  $0.0 < x < 0.12$  and a typical pyrolite [21] consisting of 20–30 V% of magnesium wüstite,  $(\text{Mg}_{(1-y)}, \text{Fe}_y)\text{O}$ , with  $1 < y/x < 4$ . The effect of Fe on the elasticity of perovskite was calculated at  $T = 0$  K [19] and is assumed to be  $T$

independent. The effect of Fe on the elasticity of magnesium wüstite is assumed to be that determined at room temperature [20] (see the Fig. 3 caption). The major difference between the two mineralogical models is the overall smaller *pyrolitic*  $K_S$  which agrees reasonably well with  $K_S^{\text{PREM}}$  in the upper part of the LM (down to  $\approx 1400$  km depth or 55 GPa). Both models describe  $G^{\text{PREM}}$  reasonably well in the upper LM for reasonable ranges of  $x$  and  $y/x$ . However, regardless of the content of magnesium wüstite,  $x$ , or  $y/x$ , with increasing depth  $K_S^{\text{PREM}}$  and  $G^{\text{PREM}}$  seem to depart consistently and in opposite directions from the values predicted along this adiabatic geotherm. For depth greater than  $\approx 1400$  km,  $K_S$  and  $G$  develop pressure gradients that are slightly larger and somewhat smaller than PREM's, respectively. Modification of the geotherm would alter  $K_S$  and  $G$  simultaneously in the same direction. Inclusion of possible anelastic effects [22] will make it even more difficult to reconcile  $G^{\text{PREM}}$  with values of  $G$  predicted for reasonable geotherms and compositions in this range. The elasticity of other phases, such as  $\text{CaSiO}_3$  [23] that could be present by up to about 5 V%, or  $\text{Al}_2\text{O}_3$  [24,25] which forms a solid solution with  $\text{MgSiO}_3$ , must also be investigated in greater detail before a more precise conclusion can be reached. However, unless their elastic behaviors differ considerably from  $\text{MgSiO}_3$ 's, particularly their pressure and temperature gradients, current results suggest that the deep and the shallow LM differ somehow. This might be the faint spherically averaged signature of low contrast, diffuse, and wide topography boundaries in the middle of the mantle [9,10] resulting from changes in mineral composition, subtle phase changes [23,26], including those involving substitution mechanisms [25], rheology, anisotropy, or a combination of all in a perovskite-dominated LM. Its upper part behaves as a typical pyrolitic aggregate, likewise the upper mantle. However, below a certain depth that we loosely place at  $\approx 1400$  km, models encompassed by those considered here seem less adequate. This result may be viewed as evidence in support of radially heterogeneous LM models.

This research was supported by EAR-9973130, EAR-0135533, and EAR-0230319. This calculation was performed with the PWSCF package [27]. Computations were performed at the Minnesota Supercomputing Institute. S. d. G. and M. C. acknowledge partial support by MIUR under the PRIN initiative and by "Iniziativa Trasversale Calcolo Parallelo" of INFN.

- 
- [1] R. M. Wentzcovitch, J. L. Martins, and G. D. Price, *Phys. Rev. Lett.* **70**, 3947 (1993).
  - [2] B. B. Karki *et al.*, *Science* **286**, 1705 (1999); *Phys. Rev. B* **61**, 8793 (2000).
  - [3] B. B. Karki *et al.*, *Geophys. Res. Lett.* **14**, 2699 (2001); *Phys. Rev. B* **62**, 14750 (2000).
  - [4] A. R. Oganov, J. P. Brodholt, and G. D. Price, *Nature (London)* **411**, 934 (2001); *Earth Planet. Sci. Lett.* **184**, 555 (2001).

- [5] A. Yeganeh-Haeri, *Phys. Earth Planet. Inter.* **87**, 111 (1994).
- [6] Y. D. Sinelnikov *et al.*, *Science* **281**, 677 (1998).
- [7] The solidus temperature for a typical LM aggregate and the melting temperatures ( $T_M$ ) of individual mantle components are summarized in A. Zerr, X. Diegler, and R. Boehler, *Nature (London)* **281**, 243 (1998). For  $\text{MgSiO}_3$  the melting temperature varies from  $3500 < T_M < 5000$  throughout the LM. Its Debye temperature ( $T_D$ ) can be inferred from specific heat calculations ( $\approx 1100 < T_D < 1400$ ) [3].
- [8] A. D. Dziewonski and D. L. Anderson, *Phys. Earth Planet. Inter.* **25**, 297 (1981).
- [9] D. L. Anderson, *Int. Geol. Rev.* **44**, 97 (2002); *Science* **293**, 2016 (2001).
- [10] L. H. Kellogg, B. H. Hager, and R. D. Van der Hilst, *Science* **283**, 1881 (1999).
- [11] Details and methods used in this work are the same as those used in Refs. [2,3]. The nine elastic constants required free energy calculations for at least fifteen strained configurations at each  $P, T$ . The magnitude of applied strains was 0.01. The vibrational density of states was sampled at 27 (64) points throughout the irreducible Brillouin zone of the orthorhombic (monoclinic) geometry. Phonon frequencies were obtained using density functional perturbation theory [S. Baroni *et al.*, *Rev. Mod. Phys.* **73**, 515 (2001)]. Elastic moduli obtained at  $\approx 5$  GPa and 300 K agree best with those measured at ambient conditions [5]. Results from static LDA calculations in general offer volumes and compressibilities smaller than experiments. Inclusion of zero point motion energy ( $E_{zp}$ ) changes this trend substantially: increases volume and compressibility [2,3]. The combined results of LDA and  $E_{zp}$  is counteracted by shifting results by  $\approx 5$  GPa (see the Fig. 2 caption).
- [12] F. Marton and R. Cohen, *Phys. Earth Planet. Inter.* **134**, 239 (2002).
- [13] J. M. Brown and T. J. Shankland, *Geophys. J. R. Astron. Soc.* **66**, 579 (1981).
- [14] N. Funamori *et al.*, *J. Geophys. Res.* **101**, 8257 (1996).
- [15] C. R. S. da Silva *et al.*, *Phys. Earth Planet. Inter.* **118**, 103 (2000).
- [16] J. P. Watt *et al.*, *Rev. Geophys. Space Phys.* **14**, 541 (1976).
- [17] Y. Wang and D. J. Weidner, *Pure Appl. Geophys.* **146**, 533 (1996).
- [18] R. M. Wentzcovitch *et al.*, *Earth Planet. Sci. Lett.* **164**, 371 (1998).
- [19] B. Kiefer, L. Stixrude, and R. M. Wentzcovitch, *Geophys. Res. Lett.* **29**, 14683 (2002), and references therein.
- [20] I. Jackson, *Geophys. J. Int.* **134**, 291 (1998).
- [21] A. E. Ringwood, *Composition and Petrology of the Earth's Mantle* (McGraw-Hill, New York, 1975).
- [22] S. Karato, *Geophys. Res. Lett.* **20**, 1623 (1993); S.-i. Karato and B. B. Karki, *J. Geophys. Res.* **106**, 21771 (2001).
- [23] A.-H. Shim *et al.*, *Geophys. Res. Lett.* **29**, 16148 (2002).
- [24] J. Zhang and D. J. Weidner, *Science* **284**, 782 (1999).
- [25] A. Navrotsky *et al.*, *J. Geophys. Res.* **108**, 2330 (2003).
- [26] J. Badro *et al.*, *Science* **300**, 789 (2003).
- [27] PWSCF package is available at <http://www.pwscf.org>.